Journal of Solid State Chemistry 184 (2011) 1909–1914

Contents lists available at ScienceDirect

Journal of Solid State Chemistry

journal homepage: www.elsevier.com/locate/jssc

Functionalized bimodal mesoporous silicas as carriers for controlled aspirin delivery

Lin Gao, Jihong Sun*, Yuzhen Li

Department of Chemistry and Chemical Engineering, College of Environmental & Energy Engineering, Beijing University of Technology, Beijing 100124, PR China

ARTICLE INFO

Article history:
Received 20 January 2011
Received in revised form
22 April 2011
Accepted 29 May 2011
Available online 6 June 2011

Keywords:
Bimodal mesoporous silicas
Aspirin
Controlled release
Functionalization

ABSTRACT

The bimodal mesoporous silica modified with 3-aminopropyltriethoxysilane was performed as the aspirin carrier. The samples' structure, drug loading and release profiles were characterized with X-ray diffraction, scanning electron microscopy, N_2 adsorption and desorption, Fourier transform infrared spectroscopy, TG analysis, elemental analysis and UV-spectrophotometer. For further exploring the effects of the bimodal mesopores on the drug delivery behavior, the unimodal mesoporous material MCM-41 was also modified as the aspirin carrier. Meantime, Korsmeyer–Peppas equation $f_t = kt^n$ was employed to analyze the dissolution data in details. It is indicated that the bimodal mesopores are beneficial for unrestricted drug molecules diffusing and therefore lead to a higher loading and faster releasing than that of MCM-41. The results show that the aspirin delivery properties are influenced considerably by the mesoporous matrix, whereas the large pore of bimodal mesoporous silica is the key point for the improved controlled-release properties.

1. Introduction

Since the discovery of MCM-41 family in 1990 [1,2], mesoporous silica materials have received much attention due to their excellent characteristics, such as stable mesoporous structure, high specific surface area, large pore volume, regular and adjustable nano-pore sizes and a hydrophilic surface feature [3–6]. Additionally, many researchers have focused on the application of mesoporous silicas as potential drug delivery systems owing to their non-toxic nature and good biocompatibility [7–10]. As typical mesoporous silicas, MCM-41 has been used as a carrier for several different pharmaceutical compounds such as ibuprofen [11,12], vancomycin [13], model compound fluorescein [14], diflunisal, naproxen [15], hypocrellin A [16] and aspirin [17]. Qu et al. introduced MCM-41 and SBA-15 into the adsorption of captopril and investigated their loading and release kinetics [18]. Recent researches [7,19–22] have demonstrated MCM-41-type mesoporous silica nanoparticles as an efficient stimuli-responsive controlled-release system for in-vivo biomedical applications.

However, fewer reports have focused on the application of mesoporous silicas which own three-dimensional pore networks. One of such mesoporous silicas is the cubic ordered MCM-48 which has been applied in the immobilization of protein [23] as well as the encapsulation of small molecule drugs [24]. Another mesoporous silicas TUD-1 [25], which also possessed the hierarchical interconnecting structure, was used as the carrier for ibuprofen and exhibited some excellent properties in terms of efficiency and drug loading capacity. All these reports demonstrate that the mesoporous materials with interconnecting three-dimensional pore networks have obvious advantages as drug carriers.

In this work, we report the application of bimodal mesoporous silicas (BMMs) as a drug delivery carrier. Based on the literature [26], the bimodal mesoporous structure of BMMs can be easily tailored with independently controlled small pores (~3 nm) and large pores (in the range of 15–50 nm), which could be in favor of high accessibility as well as sustainable release characteristics for ideal drug delivery. Therefore, we found a simple and effective approach to synthesize a delivery carrier for aspirin by surface modification of BMMs with 3-aminopropyltriethoxysilane (APTES). For comparison, MCM-41 functionalized with aminopropyl groups was also used as the drug carrier. Finally, their drug loading and release profiles were discussed in detail.

2. Experimental section

2.1. Chemicals

Cetyltrimethylammonium bromide commonly (CTAB) was obtained from Beijing Chemical Factory. Ammonia (25 wt%) and tetraethyl orthosilicate (TEOS) were provided by Beijing Yili Chemical

* Correspondence to: Department of Chemistry and Chemical Engineering, College of Environmental & Energy Engineering, Beijing University of Technology, 100 PingLeYuan, Chaoyang District, Beijing 100124, PR China.
Fax: +86 10 67391983.
E-mail address: jhsun@bjut.edu.cn (J. Sun).

0022-4596/$ - see front matter © 2011 Elsevier Inc. All rights reserved.
doi:10.1016/j.jssc.2011.05.052

Factory. APTES and aspirin were supplied by Alfa Aesar Company. Chloroform and ethanol were purified under reduced pressure. All the materials were all A.R. grade. Doubly distilled water was used in all experiments.

2.2. Synthesis of mesoporous silicas

BMMs were synthesized based on Sun's work [27]. The synthesis procedure was as follows: 2.6115 g CTAB was dissolved in 104 ml of distilled water until the solution became transparent. Then 8 ml of TEOS was added dropwise. Finally, 4 ml of ammonia (25 wt%) was added quickly. The mixture was stirred continuously and became progressively viscous, and eventually turned into a white gel. The resulting precipitates were filtered, washed, and dried at 120 °C for 3 h. To remove the surfactant, the solid was calcined at 550 °C for 6 h with a heating rate of 5 °C/min.

MCM-41 was prepared according to the following procedure [28]: 3.644 g of CTAB was dissolved in 100 ml of deionized water and then 10 ml of NaOH solution (1 M) was added. After stirring for 15 min, 18.6 ml of TEOS was added dropwise. Then the mixture was stirred for another 2 h. The obtained gel was poured into an autoclave with Teflon lining hermetically closed and was heated at 110 °C for 48 h. Then, the product was filtered, washed with distilled water, and dried at 120 °C. To remove the surfactant, the solid was calcined at 550 °C for 6 h with a heating rate of 5 °C/min.

2.3. Modification of mesoporous silicas

The pore surface modification of the obtained mesoporous materials was carried out by a post-treatment method: prior to the functionalization, the mesoporous silicas were dried under vacuum at 150 °C for 5 h. Then 1.0 g of mesoporous silicas were suspended in 100 ml of chloroform solution of APTES (0.06 M). The reaction mixture was stirred for 5 h at room temperature. The functionalized samples were collected by filtration, drying at 80 °C for 3 h, and denoted as N-BMMs and N-MCM-41, respectively.

2.4. Aspirin adsorption and release

Aspirin (0.05 g) was firstly dissolved in ethanol (50 ml), and then N-BMMs (or N-MCM-41) (0.2 g) were added into the prepared aspirin solution. The mixture was stirred for 14 h. During the period of stirring process, 5 ml of the mixture was taken out every detecting time point, then filtered by using Nylon Filter Membranes (pore size of around 450 nm, Agilent) and washed with 5 ml ethanol to remove the Aspirin adsorbed on the outer surface of N-BMMs (or N-MCM-41). The resulting samples were denoted as A/N-BMMs (or A/N-MCM-41). The filtrate was analyzed with UV–vis absorption spectroscopy, by monitoring the major peak at 223 nm. The amount of the drug adsorbed on the adsorbent was calculated based on the mass balance before and after adsorption [11].

The release profile was obtained by soaking 0.1 g of the drug-loaded carrier in 50 ml of distilled water at room temperature, and the solution was kept stirring during the experiment. Two milliliter of solution was taken out every detecting time point for analysis of the drug concentration with UV–vis absorption spectroscopy. The cumulative release amount of the drug was determined based on a mass balance equation [11].

2.5. Characterization

The powder X-ray diffraction (XRD) measurements were recorded using a Bruker-AXS D8 Advance X-ray diffactometer using Cu$K\alpha$ radiation (λ=0.154056 nm) source for 2θ ranging from 0.6° to 10.0° with a scanning speed of 2.0°/min at 35 KV and 20 mA. The scanning electron microscopy (SEM) images were captured on a Hitachi field-emission scanning electron microscope (S-4300) operated at an accelerating voltage of 15 kV. Transmission electron microscopy (TEM) was performed on a Tecnai F20 at 200 kV. A Shimadzu UV-2450 spectrophotometer was used to measure the amount of aspirin adsorbed and released from the samples. The Fourier transform infrared (FT-IR) spectra of mesoporous silicas before and after modification were observed on a Bruker Tensor 27 analyzer. N_2 adsorption and desorption isotherms at −196 °C were obtained using a Micromeritics Tristar II. Before nitrogen adsorption, the samples were pretreated for 5 h under helium at 150 °C for BMMs and MCM-41, 120 °C for modified samples and 80 °C for drug-loaded samples. The isotherm data were analyzed with BET (Brunauer–Emmett–Teller) and the plots of the corresponding pore size distribution were obtained from the desorption branches of the isotherms by using BJH (Barrett–Joyner–Halenda) model. Thermogravimetric analyses (TGA) were carried out between 25 and 800 °C using a Perkin-Elmer Pyris 1 TG analyzer under 100 ml/min N_2 flow with a heating rate of 10 °C/min. The elemental compositions of the samples were analyzed by varioEL superuser.

3. Results and discussion

3.1. Characterization of mesoporous silicas

The SEM image, as depicted in Fig. 1, shows that the typical BMMs possesses nanosized spherical morphology, and the corresponding particle size distribution is found to be very narrow with a size of around less than 50 nm in Fig. 1A. However, MCM-41 is with irregular bulk powder in Fig. 1B. The representative small angle XRD patterns of the three samples are shown in Fig. 2. Before modification (Fig. 2A-a), the XRD pattern of BMMs clearly exhibited two reflections in the 2 theta range 2–10°, indexed for (1 0 0) and (1 1 0) peaks, respectively, which can be associated with a worm-hole mesostructure. However the peak (1 1 0) was not obvious because of the fact that the peak (1 0 0) was very broad with high intensity.

After attaching –NH_2 groups onto the surface of the BMMs, for N-BMMs (Fig. 2A-b), the (1 0 0) peak intensity decreasing and its position shifting from 1.84° to 2.04° (2θ) indicate the mesoporous structure somewhat disordered and the corresponding value of d space decreased from 4.80 to 4.32 nm, suggesting that the introduction of functional groups onto the BMMs mesostructure has a remarkably disruptive effect caused by the condensation between siloxane and functional groups during the modification process [29]. The XRD pattern of A/N-BMMs, as seen in Fig. 2A-c, shows that the (1 0 0) peak is still present, indicating that the mesoporous framework was maintained after the loading process, while the diffraction peak intensity decreased and its position shifted slightly with comparison of BMMs.

The XRD patterns of modified and aspirin loaded MCM-41 (Fig. 2B) also presented similar change trends, that the (1 0 0) peak intensity decreased and its position shifted to low 2θ angle with the introduction of –NH_2 groups and aspirin molecules into the mesopores of BMMs. The results are consistent with other previous reports [30].

N_2 adsorption–desorption isotherms and corresponding pore size distribution of samples are shown in Fig. 3. Their detailed textural results are summarized in Table 1. The N_2 isotherms of BMMs, N-BMMs and A/N-BMMs all exhibited two inflections: the first inflection occurred in a relative pressure range from 0.30 to 0.50 and the second one, much steeper, appeared at relative pressures ranging from 0.80 to 0.98, as can be seen in Fig. 3A,

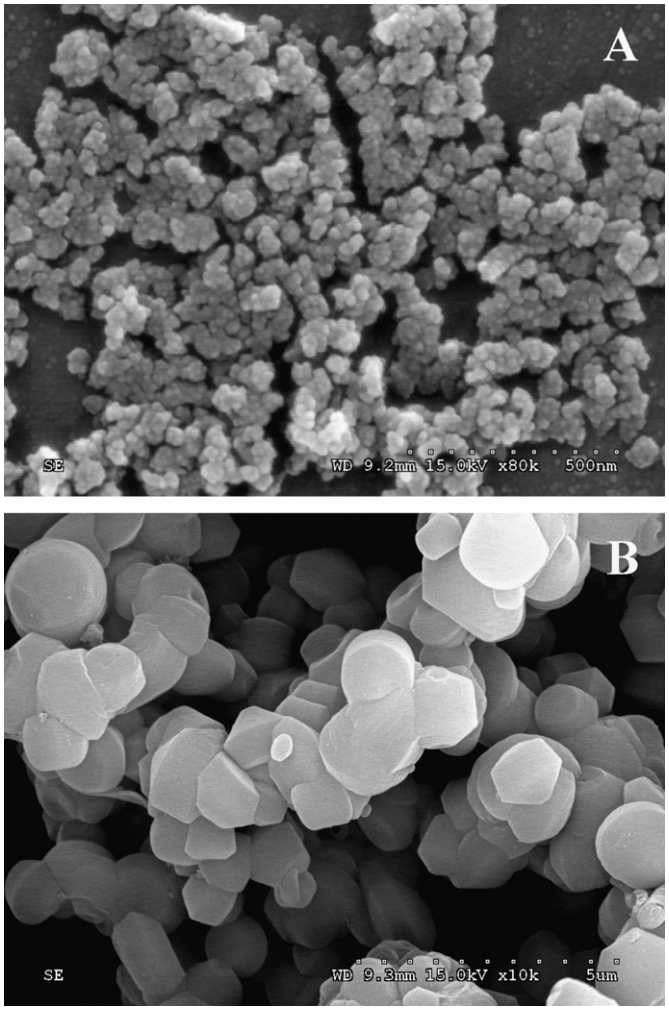

Fig. 1. SEM images of a typical BMMs (A) and MCM-41 (B).

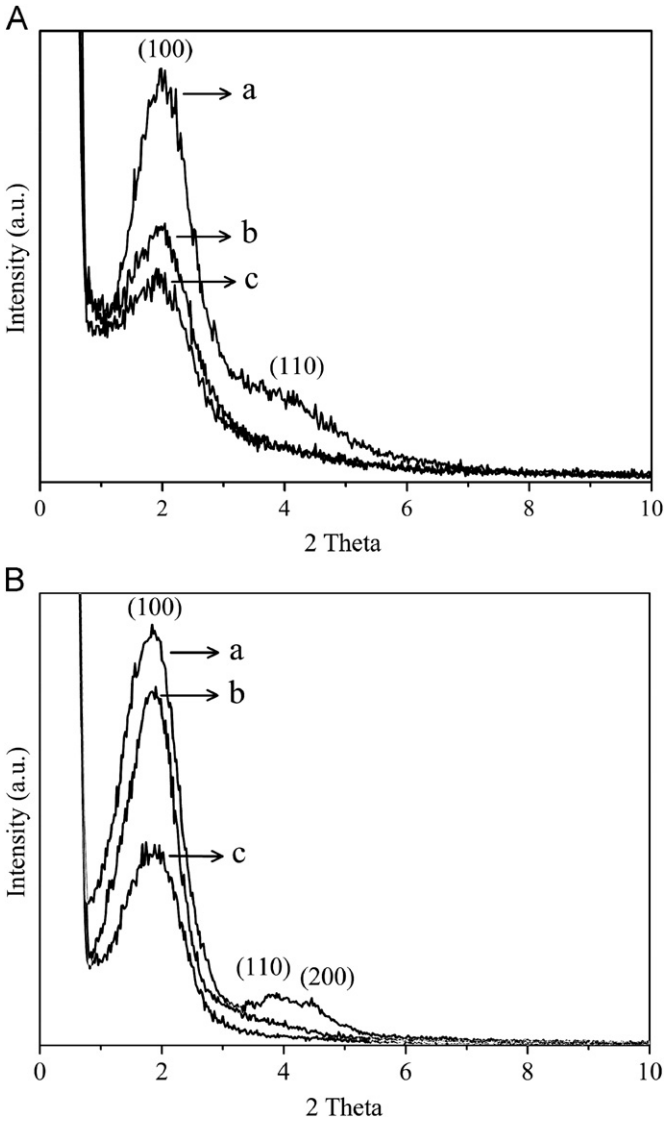

Fig. 2. XRD patterns of (A) BMMs (a), N-BMMs (b) and A/N-BMMs (c); and (B) MCM-41 (a), N-MCM-41 (b) and A/N-MCM-41 (c).

along with the corresponding pore size distribution (inserted in Fig. 3A) verifying the existence of the two pore distribution with a narrow small pore distribution around 2.88 nm and a large pore distribution around 23.6 nm, respectively. The BMMs (Fig. 3A-a) exhibited values of BET specific surface area and pore volume equal to 959 m^2/g and 2.0 cm^3/g, respectively. After modification with amino groups and adsorption of aspirin, N_2 isotherms of N-BMMs (Fig. 3A-b) and A/N-BMMs showed lower values of BET specific surface area and pore volume (526 m^2/g and 1.2 cm^3/g for N-BMMs, and 488 m^2/g and 0.8 cm^3/g for A/N-BMMs, respectively), suggesting the presence of amino moieties on the mesopore surface and successful adsorption of aspirin molecules in the mesopore channels. These results were further confirmed by the observation from their pore size distribution (inserted in Fig. 3A). After the introduction of amino groups, the small mean pore size of N-BMMs decreased to 2.54 nm, and for A/N-BMMs the small mean pore size was smaller than 2.06 nm.

For MCM-41, N-MCM-41 and A/N-MCM-41(Fig. 3B), it is obvious that the surface area and pore volume also decreased gradually. And the detailed information is presented in Table 1.

The TEM image of BMMs in Fig. 4 confirms the presence of a large number of narrow pores with a size of 3 nm and also the spherical morphology of BMMs. Combined with the above observation of pore size distribution from N_2 adsorption and desorption isotherms, the TEM image can further verify the accumulation of the spherical particles of BMMs, which led to the appearance of the large pore around 24 nm. The TEM image of the N-BMMs (not shown) shows a similar observation, indicating that the post-treatment procedure has no strong influence on the morphology and pore structure of BMMs.

Fig. 5 shows the FT-IR spectra of four different samples. As can be seen in Fig. 5a, for the BMMs, the bands at 1080, 792 and 445 cm^{-1} are attributed to the stretching vibrations of the mesoporous framework (Si–O–Si) [31]. Comparatively for the N-BMMs, the appearance of two new bands at 773 and 1417 cm^{-1} in Fig. 5b can be assigned to the stretching vibration of Si–O–C and the asymmetrical stretching of C–N [32], respectively, originating from the $-Si-O-(CH_2)_3-NH_2$ group of APTES after the modification. These results show that the functional groups have been successfully grafted on the pore surface of BMMs.

For the aspirin loaded N-BMMs, four new characteristic absorption peaks at 1604, 1571, 1492 and 1467 cm^{-1} (Fig. 5c) are ascribed to the skeletal vibration of phenyl, in agreement with the spectrum typically observed in a pure aspirin sample (Fig. 5d). In addition, the band at 838 cm^{-1} corresponds to the C–H out-of-plane bonding vibration [33–35]. These observations confirm that aspirin was successfully loaded into the pore channels of N-BMMs.

The TG and DTG analysis of samples were carried out and the discussions were presented in another paper [36].

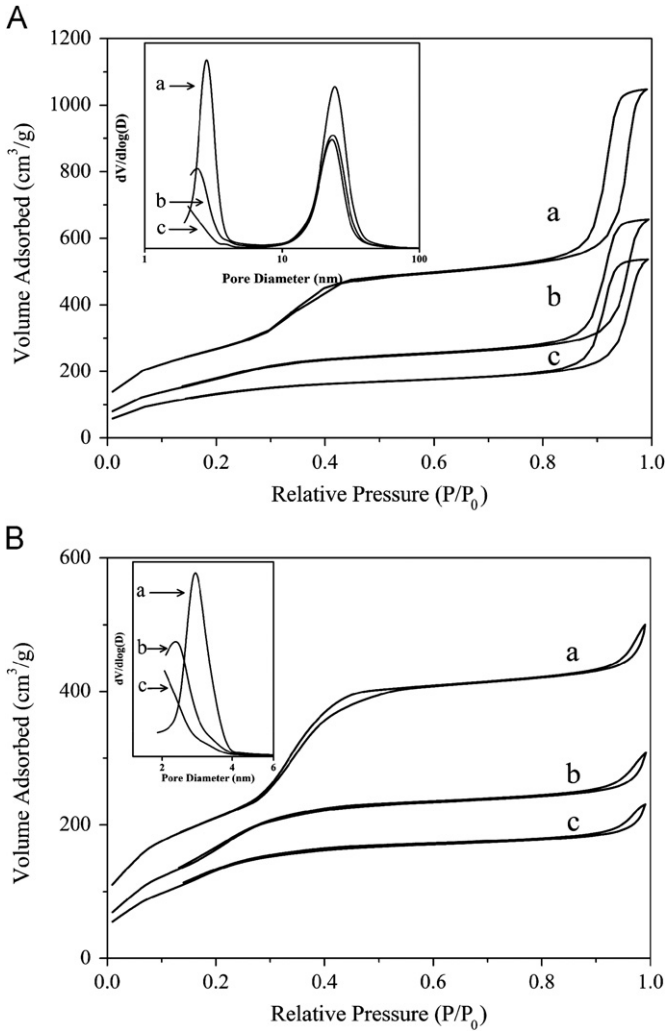

Fig. 3. N_2 adsorption-desorption isotherms of (A) BMMs (a), N-BMMs (b), and A/N-BMMs (c); (B) MCM-41 (a), N-MCM-41 (b) and A/N-MCM-41 (c) and their corresponding plots of the pore size distribution (inserted).

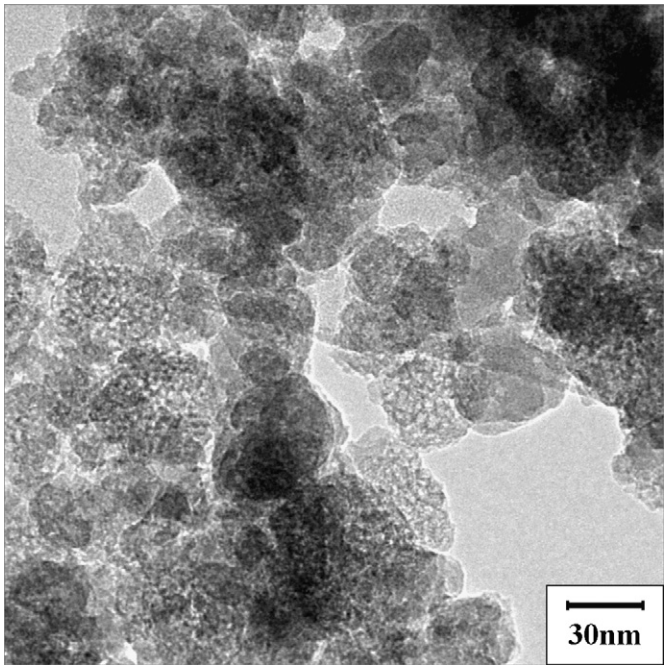

Fig. 4. TEM micrograph of a typical BMMs.

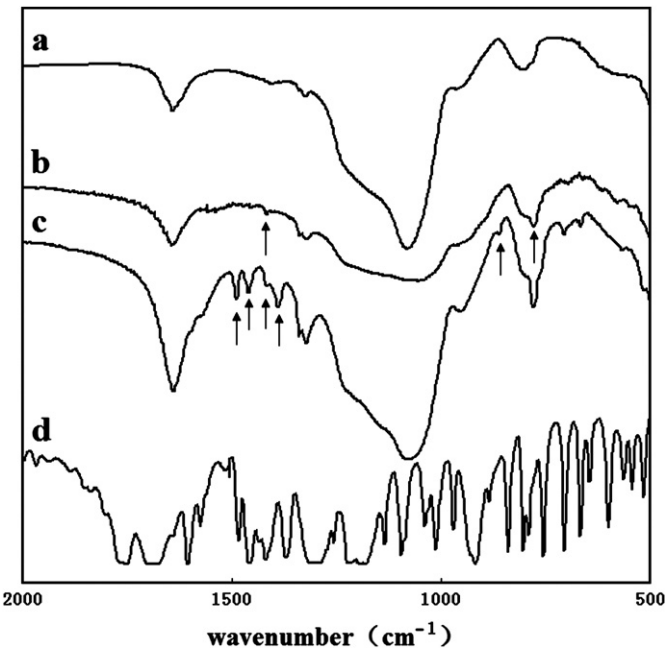

Fig. 5. FT-IR spectra of BMMs (a), N-BMMs (b), A/N-BMMs (c) and pure aspirin (d).

Table 1
Textural properties of relative samples.

Samples	BET surface area (m^2/g)	Pore volume (cm^3/g)	Small mean pore (nm)	Large mean pore (nm)
BMMs	959	2.0	2.88	23.6
N-BMMs	526	1.2	2.54	23.8
A/N-BMMs	488	0.8	< 2.06	20.7
MCM-41	771	0.8	2.73	
N-MCM-41	704	0.5	2.37	
A/N-MCM-41	513	0.3	< 2.04	

Besides, elemental compositions of the samples were provided in Table 2. It shows that the N content (wt%) of both N-BMMs and N-MCM-41 clearly increased from zero (before modification) to around 2 after modification with 3-aminopropyltriethoxysilane (APTES) and the C/N molar ratio was around 3.5, which was almost consistent with that of 3-aminopropyl groups (the C/N molar ratio is 3). Meanwhile, after drug adsorption, the C content (wt%) of both A/N-BMMs and A/N-MCM-41 obviously increased from 6.692/6.946 (before adsorption) to around 11, strongly proved the successful adsorption of drug molecules.

Table 2
Elemental composition of samples.

Samples	N content (wt%)	C content (wt%)
BMMs	0	0.314
N-BMMs	2.036	6.692
A/N-BMMs	1.846	11.05
MCM-41	0	0.240
N-MCM-41	2.440	6.946
A/N-MCM-41	2.102	11.36

The MCM-41 samples, before and after $-NH_2$ modification and aspirin loading, were also characterized with the TEM and TG. The TEM images and TG results confirmed the stability of the ordered mesoporous structure of MCM-41 series samples and indicated the successful modification and aspirin loading, which are consistent with previous reports [29].

3.2. Adsorption of aspirin

It has been reported that the chemical properties of the mesoporous surface and relative mesoporous size might greatly influence the loading profiles of guest molecules in the mesoporous silica [37]. The effects of functional groups and pore network of mesoporous silica on aspirin loading process have been investigated in our group [38]. And some other reports also verified the protonated aminopropyl groups ($-NH^{3+}$) grafted on the surface of mesoporous materials act as attraction centers for carboxyl groups (–COOH) of aspirin molecules, and the resulting electrostatic interaction appears to be significant factors influencing the drug loading capacity of mesoporous materials [30,34,37]. Fig. 6 shows the uptake curves of aspirin loaded in the mesoporous silicas. The results show that the uptake profiles of aspirin in N-BMMs and N-MCM-41 are very similar, and both take about 2.0 h to reach the equilibrium (Fig. 6). This may be due to the fact that both materials have similar small pore channels where mass transfer limitations are available for aspirin diffusion [30,33,36,38,39].

However, the aspirin loading capacity on the N-BMMs is significantly different from N-MCM-41. The N-BMMs (Fig. 6a) has an aspirin loading of 20.5 mg/0.2 g carrier, which is much higher than that on the N-MCM-41 (11.6 mg/0.2 g carrier) (Fig. 6b). Based on the results of N_2 adsorption and desorption and the elemental analysis, although the surface area of N-MCM-41 is larger than that of N-BMM and N contents associated to amino groups is higher as well, the loading amount of N-BMMs was more than that of N-MCM-41, the most reason is ascribed to the different morphology of BMMs from MCM-41. Apparently, N-BMMs possess spherical morphology with large numbers of short small pores around 3.0 nm, while MCM-41 with irregular bulk powder is of long and one-dimensional mesopores around 3.0 nm. Comparably, the short mesopores of BMMs is better for the diffusion of aspirin in the mesoporous channels than MCM-41, for which the drug molecule were mainly adsorbed or accumulated at the pore openings and the total drug loading amount is less than that of N-BMMs. These results suggest that the drug loading capacity could be improved by using a bimodal mesoporous material with functionalized pore walls.

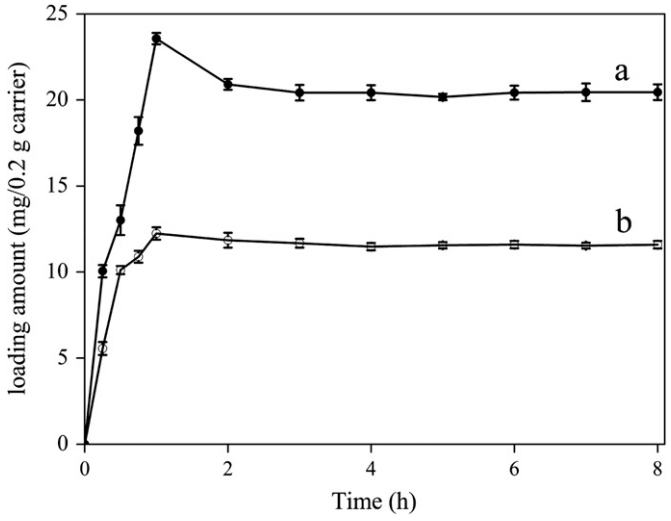

Fig. 6. Loadings of aspirin in the N-BMMs (a) and the N-MCM-41 (b).

3.3. Drug release profiles

Fig. 7 shows drug release profiles from A/N-BMMs and A/N-MCM-41 in distilled water. Obviously there is a release burst in 1 h of both systems, which should be ascribed to the fast dissolution of aspirin from the outer surface of carrier initially. Then, as the aspirin concentration in the release solution gradually increased, some of the desorbed aspirin molecules partially re-adsorbed onto the carrier surface via weak physical interaction (dynamic equilibrium process) between the aspirin molecules and surface hydrophilic groups of carries. This phenomenon has no direct contact with the controlled release in the following time, so these points were neglected in the statistical comparison. In Fig. 7A-a, the A/N-BMMs delivery system exhibits 40 wt% of drug in the initial release stage within 3 h, 80 wt% was released within 9 h, and the release process nearly stopped over a period of 12 h. In comparison, however, for A/N-MCM-41, only 30 wt% is released within 3 h, and it takes more than 12 h to reach 70 wt%,

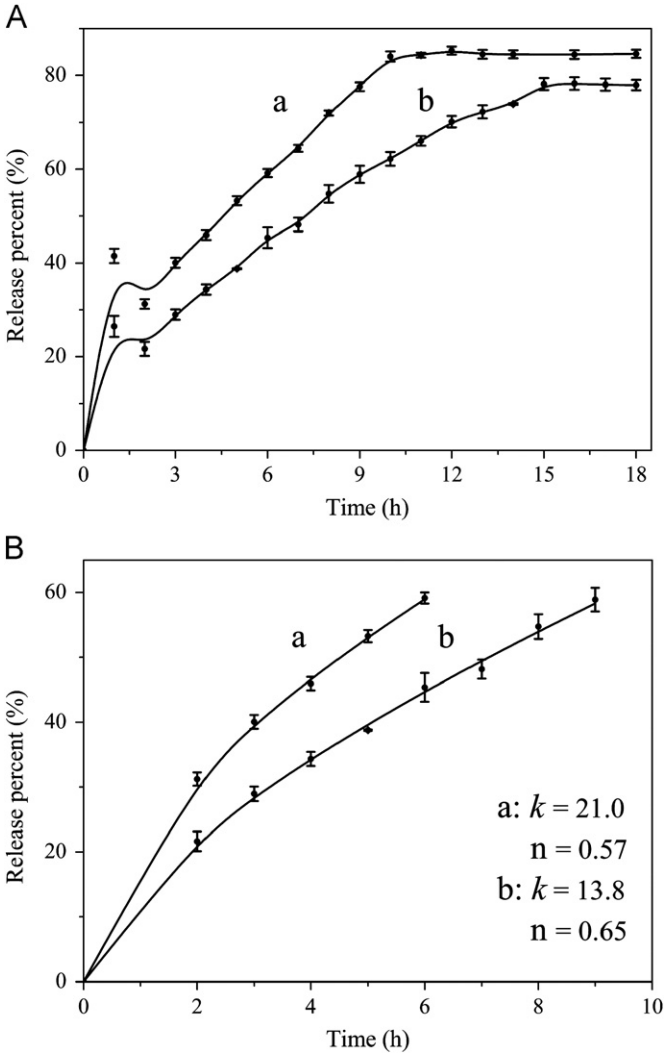

Fig. 7. Aspirin release profiles (A) and the initial 60 wt% of aspirin release fitted with the Korsmeyer–Peppas model $f_t = kt^n$ (B). A/N-BMMs (a) and A/N-MCM-41 (b) in distilled water.

and the release kept for more than 16 h (Fig. 7A-b). Obviously, it is noted that the drug release rate from N-BMMs is much faster than that from N-MCM-41, especially during the period time from 3 to 12 h. The difference in aspirin release rate might be due to the diverse pore network of BMMs and MCM-41 [25,33,40]. Generally, large pore channel might reduce steric diffusion resistance, and therefore the drug release from N-BMMs carrier through an additional large pore (23.6 nm, besides 2.88 nm) was more freely than that from N-MCM-41 carrier which has only one small pore size (2.7 nm), which was in agreement with previous reported literatures [23]. In order to compare the aspirin release characteristics of the functionalized mesoporous silica carriers with different mesopores network in detail and then to give explanation for the above finding, the dissolution data was fitted with a simple, semi-empirical model: the Korsmeyer–Peppas equation [41]: $f_t = kt^n$, where f_t is the fractional release of aspirin, the kinetic release constant k is related to the structural and geometrical characteristics of the carrier, t is the elapsed time and the release exponent n describes the aspirin release mechanism. In such case, the faster release of aspirin from the N-BMMs carrier (kinetic constant $k=21.0$) compared to N-MCM-41 ($k=13.8$) indicated the unrestricted diffusion, due to the high accessibility of the bimodal mesoporous network. On the other hand, the release exponent n of N-BMMs carrier and N-MCM-41 carrier were 0.58 and 0.65, respectively, suggesting that the aspirin release mechanism of the BMMs carrier was more diffusion based than that of the MCM-41 carrier [25]. These results demonstrated that the highly accessibility of the bimodal mesoporous network of BMMs provided a relatively unrestricted release of the drug, whereas the uniform mesoporous pathways of the MCM-41 sterically hindered the free diffusion of the drug from the mesopores.

4. Conclusion

The bimodal mesoporous silica with the small and large pore size distributions centralized at 2.9 and 24 nm, respectively, has been synthesized and used as carriers for aspirin loading and release. The characterization results show that the typical BMMs have a microsized spherical morphology with a uniform size of around 50 nm in diameter and possess bimodal mesopore structure. The synthesized N-BMMs has a higher loading for aspirin and a much faster drug release rate, compared to that of the N-MCM-41, implying that the existence of the large pore have great influence on the drug diffusion in the pore channel. Therefore, we concluded that bimodal mesoporous silica is a potentially useful controlled drug release carrier. In order to realize the application of modified BMMs as drug carrier, the relative research on toxicity of modified BMMs is under work in our group.

Acknowledgments

This work was supported by the National Natural Science Foundation of China (20851002, 21076003), the National Basic Research Program of China (973 Program 2009CB930200), and the Funding Project for Academic Human Resources Development in Institutions of Higher Learning under the jurisdiction of the Beijing Municipality (PHR 200907105, and 00500054R5005).

References

[1] C.T. Kresge, M.E. Leonowicz, W.J. Roth, J.C. Vartuli, J.S. Beck, Nature 359 (1992) 710–712.
[2] J.S. Beck, J.C. Vartuli, W.J. Roth, M.E. Leonowicz, C.T. Kresge, K.D. Schmitt, C.T.-W. Chu, D.H. Olson, E.W. Sheppard, S.B. McCullen, J.B. Higgins, J.L. Schlenkert, J. Am. Chem. Soc. 114 (1992) 10834–10843.
[3] D.M. Ford, E.E. Simanek, D.F. Shantz, Nanotechnology 16 (2005) S458–S475.
[4] H.D. Zhang, Y.H. Sun, K.Q. Ye, P. Zhang, Y. Wang, J. Mater. Chem. 15 (2005) 3181–3186.
[5] F.J. Brieler, P. Grundmann, M. Fröba, L.M. Chen, P.J. Klar, W. Heimbrodt, H.-A. Krug, T. Kurz, A. Loidl, Eur. J. Inorg. Chem. 18 (2005) 3597–3611.
[6] M.J. Jia, A. Seifert, M. Berger, H. Giegengack, S. Schulze, W.R. Thiel, Chem. Mater. 16 (2004) 877–882.
[7] I.I. Slowing, B.G. Trewyn, S. Giri, V.S.-Y. Lin, Adv. Funct. Mater. 17 (2007) 1225–1236.
[8] F. Balas, M. Manzano, P. Horcajada, M. Vallet-Regí, J. Am. Chem. Soc. 128 (2006) 8116–8117.
[9] S.P. Hudson, R.F. Padera, R. Langer, D.S. Kohane, Biomaterials 29 (2008) 4045–4055.
[10] Y.S. Lin, L. Haynes, J. Am. Chem. Soc. 132 (2010) 4834–4842.
[11] M. Vallet-Regí, A. Rámila, R.P. del Real, J. Perez-Pariente, J. Chem. Mater. 13 (2001) 308–311.
[12] C. Charnay, S. Bégu, C. Tourne-Peteilh, L. Nicole, D.A. Lerner, J.M. Devoisselle, Eur. J. Pharm. Biopharm. 57 (2004) 533–540.
[13] C.Y. Lai, B.G. Trewyn, D.M. Jeftinija, K. Jeftinija, S. Xu, S. Jeftinija, V.S.-Y. Lin, J. Am. Chem. Soc. 125 (2003) 4451–4459.
[14] K.A. Fisher, K.D. Huddersman, M.J. Taylor, Chem. Eur. J. 9 (2003) 5873–5878.
[15] G. Cavallaro, P. Pierro, F.S. Palumbo, F. Testa, L. Pasqua, R. Aiello, Drug Deliv. 11 (2004) 41–46.
[16] L.Z. Zhang, G.Q. Tang, B.W. Gao, G.L. Zhang, Chem. Phys. Lett. 396 (2004) 102–109.
[17] W. Zeng, X.F. Qian, Y.B. Zhang, J. Yin, Z.K. Zhu, Mater. Res. Bull. 40 (2005) 766–772.
[18] F.Y. Qu, G.S. Zhu, S.Y. Huang, S.G. Li, J.Y. Sun, D.L. Zhang, S.L. Qiu, Micro. Meso. Mater. 92 (2006) 1–9.
[19] K. Patel, S. Angelos, W.R. Dichtel, A. Coskun, Y.W. Yang, J.I. Zink, J.F. Stoddart, J. Am. Chem. Soc. 130 (2008) 2382–2383.
[20] Y.N. Zhao, B.G. Trewyn, I.I. Slowing, V.S.-Y. Lin, J. Am. Chem. Soc. 131 (2009) 8398–8400.
[21] I.I. Slowing, C.W. Wu, J.L. Vivero-Escoto, V.S.Y. Lin, Small 5 (2009) 57–62.
[22] C.H. Lee, S.H. Cheng, Y.J. Wang, Y.C. Chen, N.T. Chen, J. Souris, C.T. Chen, C.Y. Mou, C.S. Yang, L.W. Lo, Adv. Funct. Mater. 19 (2009) 215–222.
[23] L. Washmon-Kriel, V.L. Jimenez, K.J. Balkus Jr, J. Mol. Catal. B: Enzymatic 10 (2000) 453–469.
[24] I. Izquierdo-Barba, Á. Martinez, A.L. Doadrio, J. Perez-Pariente, M. Vallet-Regí, Eur. J. Pharm. Sci. 26 (2005) 365–373.
[25] T. Heikkilä, J. Salonen, J. Tuura, M.S. Hamdy, G. Mul, N. Kumar, T. Salmi, D.Yu. Murzin, L. Laitinen, A.M. Kaukonen, J. Hirvonen, V.-P. Lehto, Int. J. Pharm. 331 (2007) 133–138.
[26] J.H. Sun, Z.P. Shan, T. Maschmeyer, M.-O. Coppens, Langmuir 19 (2003) 8395–8402.
[27] L. Gao, J.H. Sun, Acta Petrolei. Sin. B10 (2006) 265–268.
[28] W. Zeng, X.F. Qian, Y.B. Zhang, J. Yin, Z.K. Zhu, Mater. Res. Bull. 40 (2005) 766–772.
[29] X.M. Wang, X.Z. Du, C.L. Li, X. Cao, Mater. Lett. 62 (2008) 3232–3235.
[30] M. Manzano, V. Aina, C.O. Arean, F. Balas, V. Cauda, M. Colilla, M.R. Delgado, M. Vallet-Regí, Chem. Eng. J. 37 (2008) 30–37.
[31] P.P. Yang, Z.W. Quan, L.L. Lu, S.S. Huang, J. Lin, Biomaterials 29 (2008) 692–702.
[32] L. Pasqua, F. Testa, R. Aiello, S. Cundari, J.B. Nagy, Micro. Meso. Mater. 103 (2007) 166–173.
[33] F.Y. Qu, G.S. Zhu, H.M. Lin, W.W. Zhang, J.Y. Sun, S.G. Lia, S.L. Qiu, J. Solid State Chem. 179 (2006) 2027–2035.
[34] T.P.B. Nguyen, J.-W. Lee, W.Gg. Shim, H. Moon, Micro. Meso. Mater 110 (2008) 560–569.
[35] K. Sarkar, K. Dhara, M. Nandi, P. Roy, A. Bhaumik, P. Banerjee, Adv. Funct. Mater. 19 (2009) 223–234.
[36] L. Gao, J.H. Sun, L. Zhang, Y.Z. Li, B. Ren, J. Nanosci. Nanotechnol., accepted.
[37] B. Muñoz, A. Rámila, J. Perez-Pariente, I. Díaz, M. Vallet-Regí, Chem. Mater. 15 (2003) 500–503.
[38] L. Gao, J.H. Sun, Acta Petrolei. Sin. B10 (2006) 265–268.
[39] Q.L. Tang, Y.X. Chen, J.H. Chen, J. Li, Y. Xu, D. Wu, Y.H. Sun, J. Solid State Chem. 183 (2010) 73–83.
[40] C.D. Nunes, P.D. Vaz, A.C. Fernandes, P. Ferreira, C.C. Romao, M.J. Calhorda, Eur. J. Pharm. Biopharm. 66 (2007) 357–365.
[41] P. Costa, J.M.S. Lobo, Eur. J. Pharm. Sci. 13 (2001) 123–133.